1997

Three-dimensional upper crustal velocity structure beneath San Francisco Peninsula, California

Tom Parsons
U.S. Geological Survey

Mary Lou Zoback
U.S. Geological Survey, marylouz@stanford.edu

Three-dimensional upper crustal velocity structure beneath San Francisco Peninsula, California

Tom Parsons and Mary Lou Zoback

U.S. Geological Survey, Menlo Park, California

Abstract. This paper presents new seismic data from, and crustal models of the San Francisco Peninsula. In much of central California the San Andreas fault juxtaposes the Cretaceous granitic Salinian terrane on its west and the Late Mesozoic/Early Tertiary Franciscan Complex on its east. On San Francisco Peninsula, however, the present-day San Andreas fault is completely within a Franciscan terrane, and the Pilarcitos fault, located southwest of the San Andreas, marks the Salinian-Franciscan boundary. This circumstance has evoked two different explanations: either the Pilarcitos is a thrust fault that has pushed Franciscan rocks over Salinian rocks or the Pilarcitos is a transform fault that has accommodated significant right-lateral slip. In an effort to better resolve the subsurface structure of the peninsula faults, we established a temporary network of 31 seismographs arrayed across the San Andreas fault and the subparallel Pilarcitos fault at ~1–2 km spacings. These instruments were deployed during the first 6 months of 1995 and recorded local earthquakes, air gun sources set off in San Francisco Bay, and explosive sources. Travel times from these sources were used to augment earthquake arrival times recorded by the Northern California Seismic Network and were inverted for three-dimensional velocity structure. Results show lateral velocity changes at depth (~0.5–7 km) that correlate with downward vertical projections of the surface traces of the San Andreas and Pilarcitos faults. We thus interpret the faults as high-angle to vertical features (constrained to a 70°–110° dip range). From this we conclude that the Pilarcitos fault is probably an important strike-slip fault that accommodated much of the right-lateral plate boundary strain on the peninsula prior to the initiation of the modern-day San Andreas fault in this region sometime after about 3.0 m.y. ago.

Introduction

Since the 1906 San Francisco earthquake, the San Andreas and related faults have been seismically quiet on San Francisco Peninsula [*Olson and Lindh*, 1985; *Olson and Zoback*, 1992; M. L. Zoback and J. A. Olson, unpublished data, 1996]. The relative lack of earthquake hypocenters beneath the peninsula has left many unresolved questions about the subsurface geology and its relation to the structure of the San Andreas and associated faults. Surprisingly little is known about the subsurface structure of the San Francisco Peninsula because of conditions adverse to seismic techniques; the peninsula is heavily urbanized except in areas of steep, brush-covered topography. This paper presents seismic data from San Francisco Peninsula that were collected during 1995 by the U.S. Geological Survey in an effort to characterize its structure. The seismic experiments were conducted with three broad goals: (1) to conduct a general site characterization study because San Francisco Peninsula has been suggested as a possible deep drilling site into the San Andreas fault zone, (2) to enable a better seismic hazard assessment of the Pilarcitos fault, a fault of unknown subsurface geometry and sense of slip that splays off of the San Andreas fault on the Peninsula (Figure 1), and (3) to provide a three-dimensional (3-D) velocity model for San Francisco Peninsula that will enable better interpretation and location of historic and future earthquakes for use in subsequent studies.

In this paper we show new earthquake and controlled source seismic data collected on San Francisco Peninsula. Seismic travel time data were collected and modeled for 3-D velocity structure, and high-resolution refraction data were collected along a two-dimensional profile crossing the faults. We show results from inversion of travel times for upper crustal seismic velocity and interpretations of those models. By interpreting the resolvable velocity structure we demonstrate a simple kinematic model for the development of the San Andreas fault on San Francisco Peninsula and its relationship to the Pilarcitos fault.

Tectonic Setting and Geology of San Francisco Peninsula and Bay Region

The San Francisco Bay region lies within the surface expression of a broad (~70–80 km wide) plate boundary zone between the Pacific and North American plates. As a result, the region is highly deformed and faulted, and includes major seismic hazards as evidenced recently by the 1989 M7.1 Loma Prieta earthquake as well as by the 1906 M7.7 San Francisco earthquake. Plate boundary right-lateral shear takes place on the San Andreas, Rodgers Creek-Hayward, Green Valley-Concord-Calaveras, and Antioch fault systems (Figure 1) as well as numerous smaller faults distributed throughout the region. This zone of crustal shear accommodates about 4–5 cm/yr of relative motion between the Pacific and North American plates [e.g., *De Mets et al.*, 1990; *Kelson et al.*, 1992]. Continuous low-level seismic activity throughout the bay area indicates that regional deformation is ongoing.
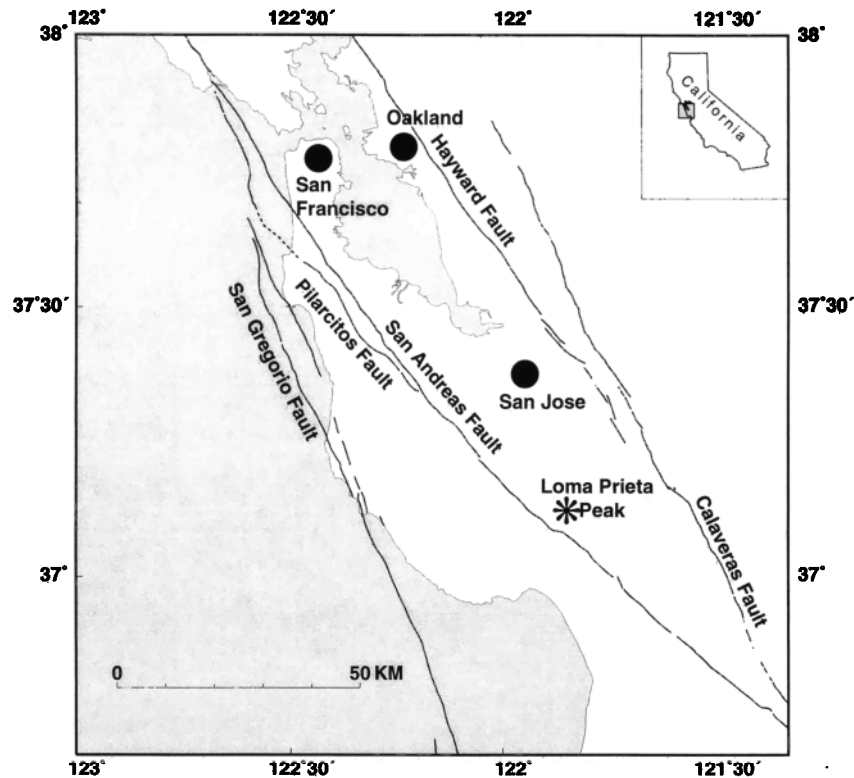
Figure 1. Tectonic setting of the San Francisco Bay region. Plate boundary slip is accommodated by right-lateral motion on the San Gregorio, San Andreas, Hayward-Rodgers Creek, Calaveras-Concord-Green Valley, and Antioch faults. This study is concentrated on San Francisco Peninsula and the San Andreas and Pilarcitos faults.

Like much of coastal California, the San Francisco Bay region is underlain primarily by the Late Mesozoic/Early Tertiary Franciscan Complex of accreted origin. This assemblage contains fragments of oceanic crust, pelagic sedimentary rocks, and land-derived marine sandstones and shales mixed together in a melange in some places, and occurring as coherent units in others [e.g., *Page*, 1992]. These rocks were emplaced during the long-term phase of oblique to head-on subduction that occurred along the California margin, and many were subsequently translated along the coast during oblique subduction and when strike-slip motion supplanted subduction during Tertiary time [e.g., *Blake*, 1984]. In general, Cretaceous granites of the Salinian terrane are exposed west of the San Andreas Fault [e.g., *Ross*, 1978] and are observed in tomographic studies to comprise much of the upper crust, butting against Franciscan rocks across the San Andreas Fault [e.g., *Foxall et al.*, 1993].
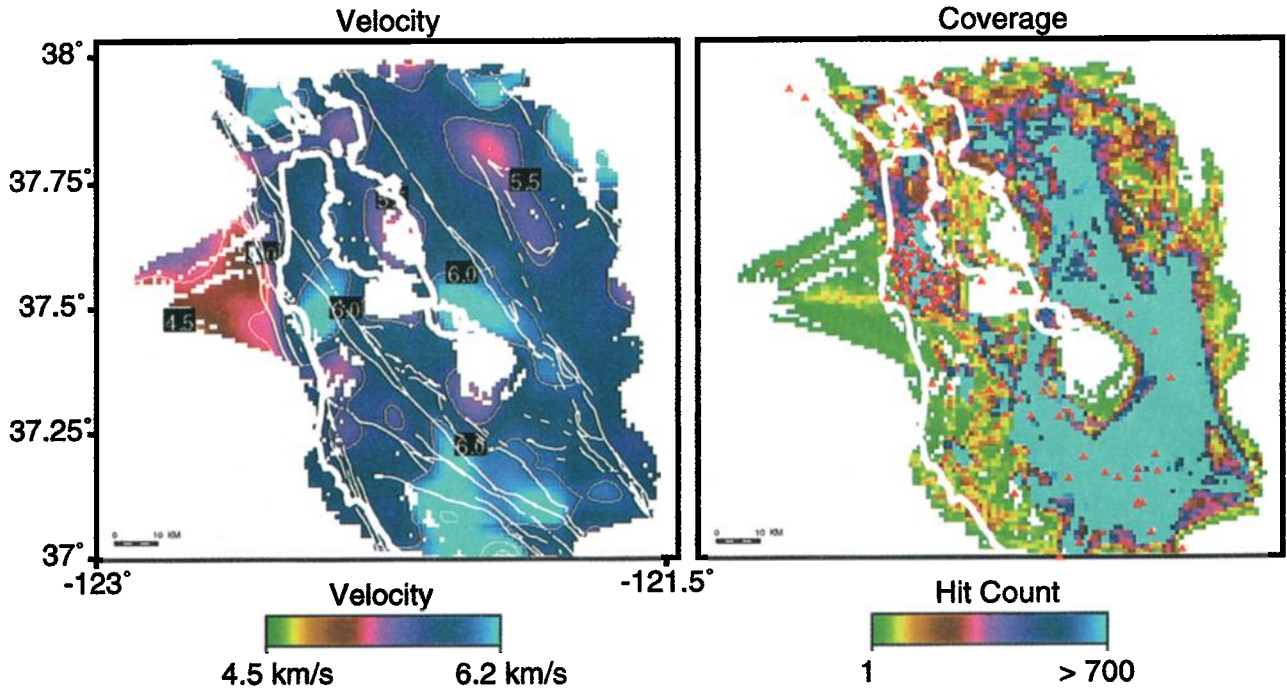
The geology of San Francisco Peninsula is dominated by the right-lateral San Andreas fault. The fault is found in a depression known geographically as the San Andreas rift zone and is bounded on its west side by the abrupt rise of the Santa Cruz Mountains. In most of central California the San Andreas fault bounds the Salinian and Franciscan terranes. On San Francisco Peninsula, however, the Salinian-Franciscan boundary is marked by the subparallel Pilarcitos fault west of the San Andreas [e.g., *Brabb and Pampeyan*, 1983] (Figure 1). On the surface, the San Andreas fault on San Francisco Peninsula is contained entirely within the Franciscan complex that locally consists of sandstones, siltstones, and shales with occasional outcrops of altered oceanic basaltic rocks (greenstone) as well

as chert and limestone. Locally, within our study area, a fragment of the Cretaceous Permanente terrane, a characteristic oceanic sequence of pillow basalts, foraminiferal limestones, and other sedimentary rocks within the Franciscan Complex is found between the Pilarcitos and San Andreas faults. Within the Permanente terrane is the distinctive Cretaceous Calera limestone that has been offset by the peninsula segment of the San Andreas fault and is used to limit the total offset to 19–23 km [e.g., *Dibblee*, 1966; *Cummings*, 1968; *Hengesh and Wakabayashi*, 1995; *McLaughlin et al.*, 1996]. The Calera limestone and Permanente terrane have not been found on the southwest side of the Pilarcitos fault and presumably have been tectonically transported beyond the present scope of observation (B. M. Page, personal communication, 1996).
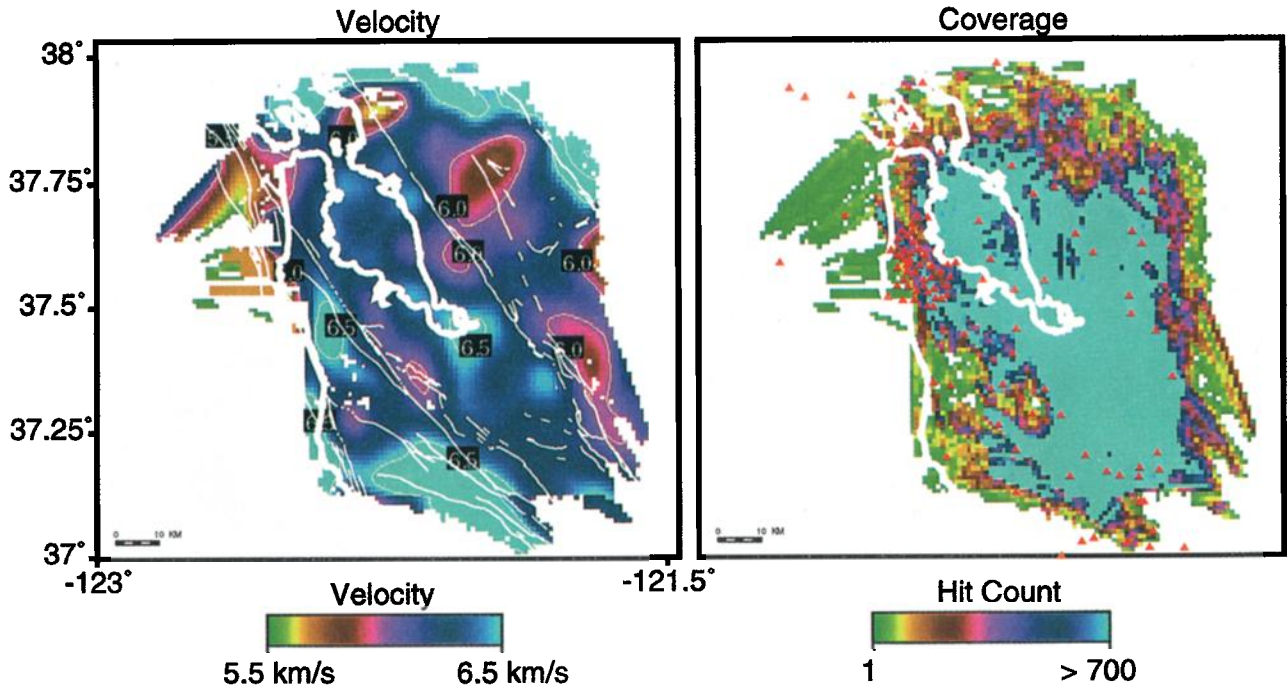
At least two possible models for the arrangement of the Salinian-Franciscan terranes on the Peninsula have been proposed: (1) the Pilarcitos fault may be an east dipping thrust fault that has emplaced Franciscan rocks over Salinian granites [e.g., *Wakabayashi and Moores*, 1988] (Figure 2a) or (2) the Pilarcitos fault may represent an old segment of the San Andreas fault system that accommodated pre-Quaternary right-lateral slip and is hence a high-angle structure [e.g., *Cummings*, 1968; *McLaughlin et al.*, 1996] (Figure 2b). The surface trace of the Pilarcitos fault has a somewhat curved or scalloped appearance (Figure 1) that makes it look more like a thrust fault than a strike-slip fault, and it is associated with east dipping mylonite fabrics indicative of shortening [*Wakabayashi and Moores*, 1988]. However, the relationship, if any, between the mylonite and the Pilarcitos fault remains unresolved.

The distinctive Calera limestone in the Franciscan complex

Plate 1. Example horizontal slices from the regional 3-D velocity model volume (3–4 and 6–7 km depth). These velocity solutions were used to apply regional earthquake sources to our detailed San Francisco Peninsula velocity model. Hole et al. (submitted manuscript, 1996) provide a detailed discussion and interpretation of regional San Francisco Bay area velocity models.

Velocity 1 km depth

Velocity 3 km depth

Velocity 5 km depth

Velocity 7 km depth

Velocity 9 km depth

Velocity 11   km depth
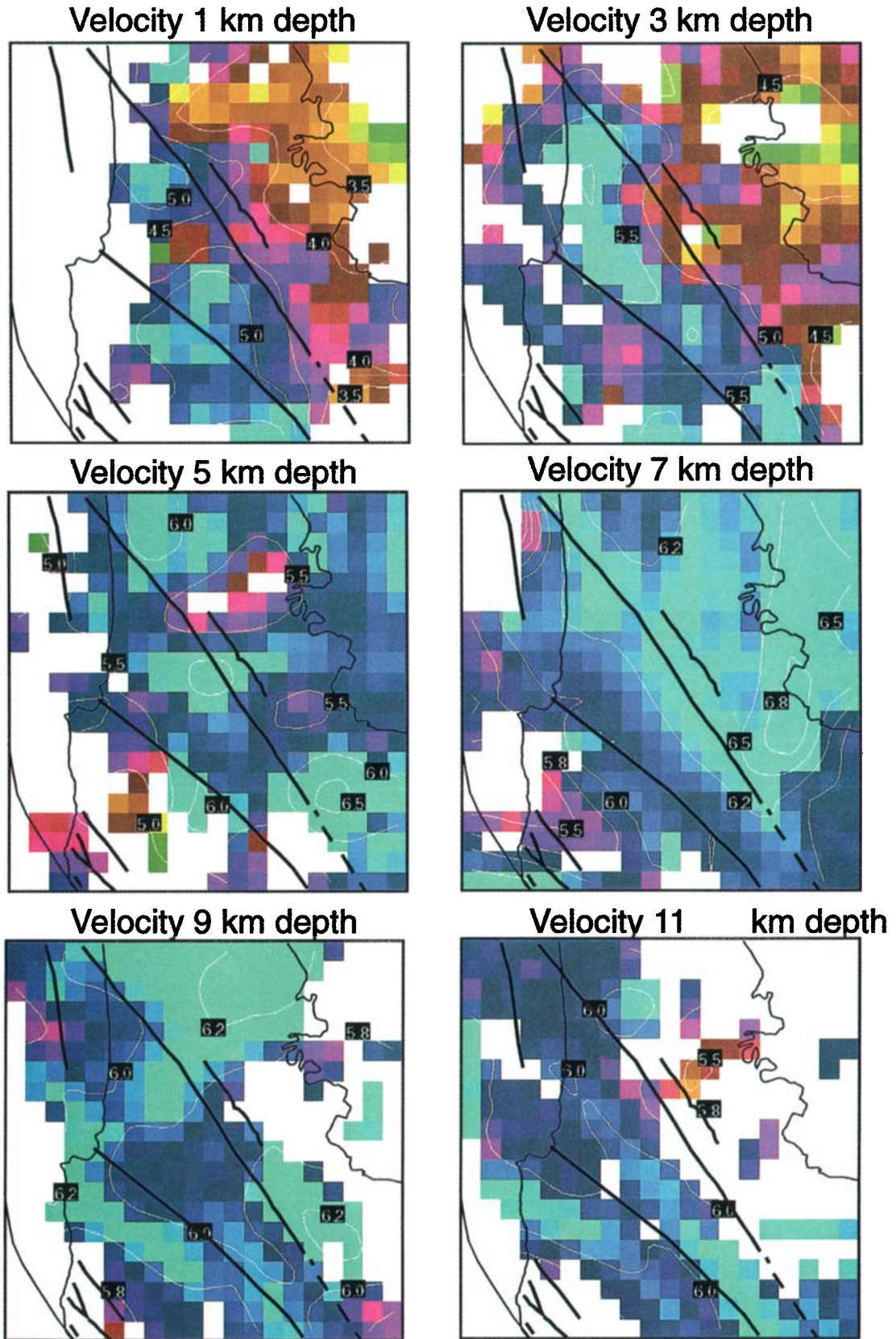
Plate 2. Horizontal slices from the 3-D San Francisco Peninsula velocity model volume from 1 to 11 km depth. The model slices represent a 20 km × 20 km area. The color scale for velocity differs from slice to slice to highlight velocity variations. Velocity values are contoured in kilometers per second. Black lines show the downward vertical projection of the surface traces of the Pilarcitos and San Andreas faults and coastlines. Features of the velocity model are discussed in the text.
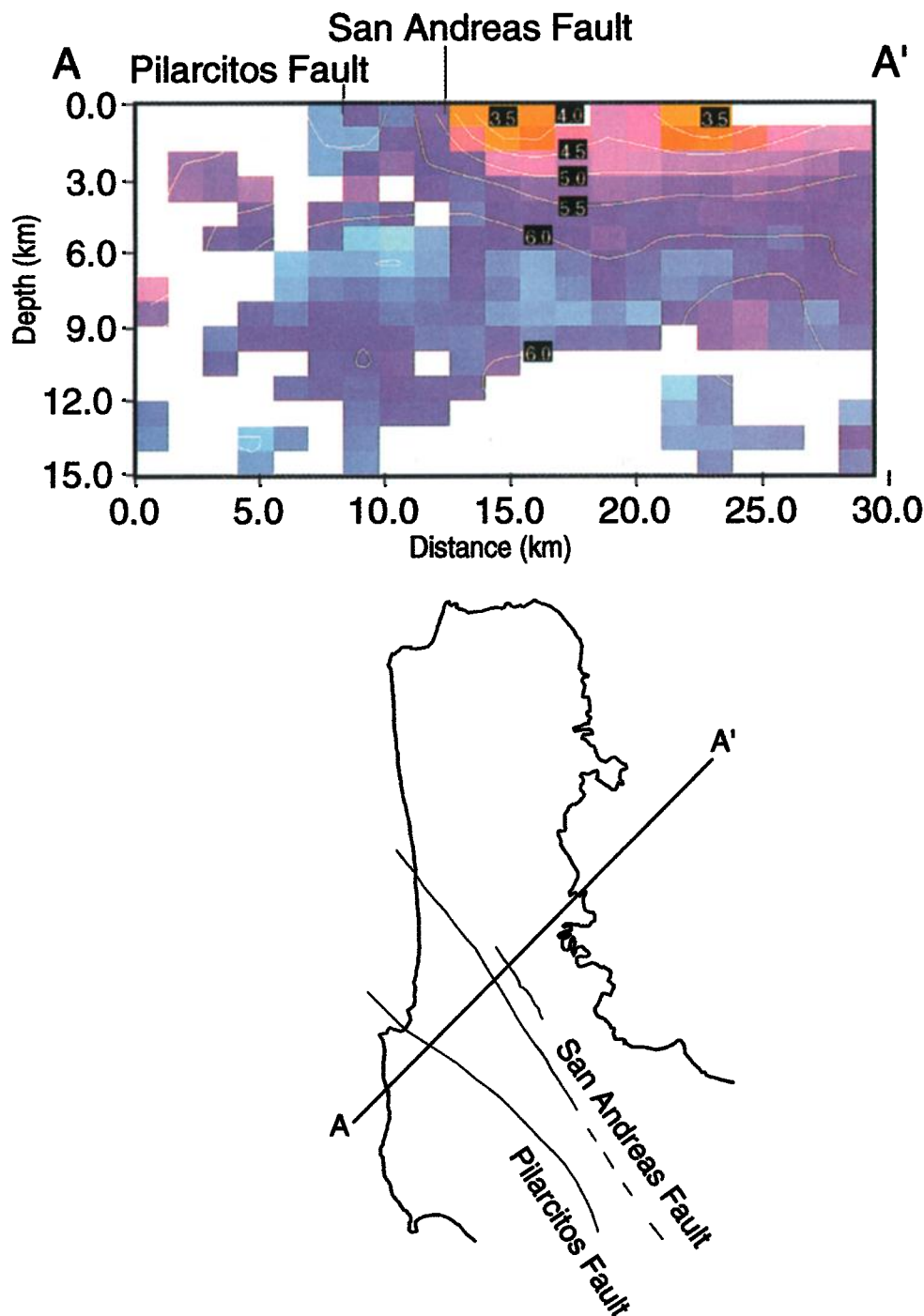
Plate 3. Example vertical slice taken from the 3-D San Francisco Peninsula velocity model volume. The cross section is oriented approximately 90° to the surface strikes of the San Andreas and Pilarcitos faults.

is offset 19–23 km by the present-day Peninsular segment of the San Andreas fault. Correlation of several distinct aeromagnetic anomalies adjacent to the San Andreas fault that act as piercing points suggests the total offset to be 23 km on the Peninsula (R. C. Jachens, personal communication, 1996). If a present-day slip rate of 15–17 mm/yr is assumed for the peninsula segment of the San Andreas fault (consistent with geodetic [*Lisowski et al.*, 1991; *Williams*, 1995] and late Holocene slip rate studies [*Hall*, 1984, 1993; *Hall et al.*, 1996], then the 23 km of total slip implies that faulting initiated between 1.3 and 1.5 Ma. However, if the averaged long-term slip rate is some-

what lower (~7–12 mm/yr post-350,000 to 400,000 years B.P.) as has been suggested by geologic studies [*Addicott*, 1969; *Cummings*, 1968; *Taylor et al.*, 1980], then an initiation time between 1.9 and 3.3 Ma can be inferred for the peninsula segment of the San Andreas fault from the observed offset.

The 1995 San Francisco Peninsula Seismic Experiment

Beginning in January 1995, we installed 31 Reftek seismographs in an array spanning San Francisco Peninsula and the
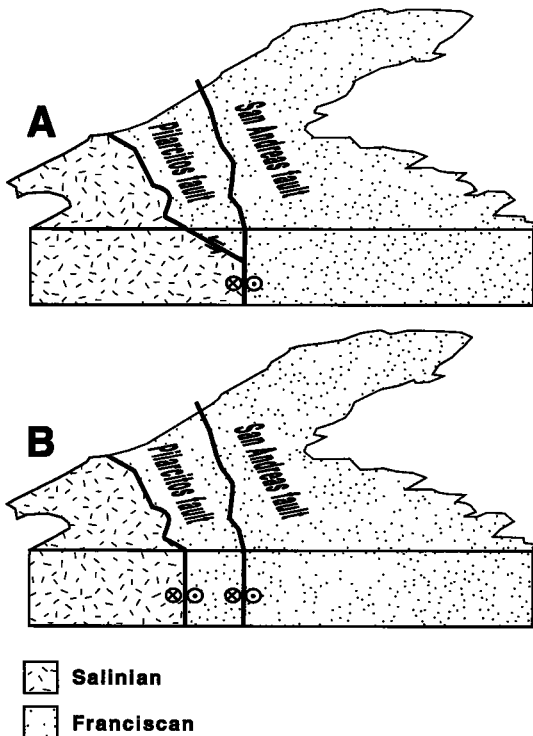
Figure 2. Simplified geology of San Francisco Peninsula and possible structural models for the relationship between the Pilarcitos and San Andreas faults. In most of central California the San Andreas fault separates the Salinian and Franciscan terranes, whereas on San Francisco Peninsula the Pilarcitos marks the terrane boundary. (a) The Pilarcitos may be an east dipping thrust fault that has pushed Franciscan rocks up over Salinian rocks, or (b) the Pilarcitos Fault may be a vertical strike-slip fault that accommodated significant right-lateral slip before the formation of the San Andreas fault on San Francisco Peninsula ~3 Ma.

San Andreas and Pilarcitos faults (Figure 3). The instruments were spaced about 1–3 km apart in any given direction and recorded continuously for 6 months. Most of the seismometers (23) were short-period (4.5 Hz) three-component sensors, an additional seven were intermediate period (1 Hz) three-component sensors, and one was a downhole broadband sensor beneath the San Mateo Bridge. These instruments each recorded an average of 105 local earthquakes (M 1.0–3.0) from January through July of 1995 (Figure 4). In April 1995 we recorded air gun sources that were detonated in San Francisco Bay (Figures 3 and 4) for vertical incidence reflection profiling [*Hart et al.*, 1995]. In June 1995 we detonated 11 chemical explosions (125–500 kg) inside and outside the network (Figure 3). The explosive sources were recorded both on the 31 Reftek seismographs and on 183 seismic group recorders (SGR) that were deployed along a southwest-to-northeast line across the Pilarcitos and San Andreas faults (Figure 3). The SGRs were deployed at 50 m spacings in a fixed array that recorded seven in-line shots spaced between 1 and 5 km apart and four fan shots located 5–20 km both north and south of the recording profile. The closely-spaced SGRs enabled us to generate a higher-resolution 2-D velocity model of the uppermost 2 km of the crust across the Pilarcitos fault.

The purpose of recording the earthquake and controlled sources was to exploit variations in the first-arrival traveltimes

(*Pg* phase) to various recording sites for use in modeling the 3-D velocity structure. By combining earthquake and controlled sources we were able to get seismic arrivals from broad offset, azimuth, and depth ranges that wouldn't have been possible with any one source mode. The use of regional earthquake sources in particular enabled deeper ray coverage for modeling than would have been possible from only a controlled source experiment because of the long offset range and deep source locations. Our study was strongly augmented by the long-term (~30 years) data catalog from the Northern California Seismic Network (NCSN) (Figure 4 shows instrument locations). By using NCSN travel time picks we were able to develop a regional 3-D velocity model of the San Francisco Bay region (Plate 1) that allowed us to treat arrivals from regional earthquakes reaching our local network as being on known travel paths (within a margin of error). There will be further discussion of the techniques applied to the travel time data in subsequent sections.
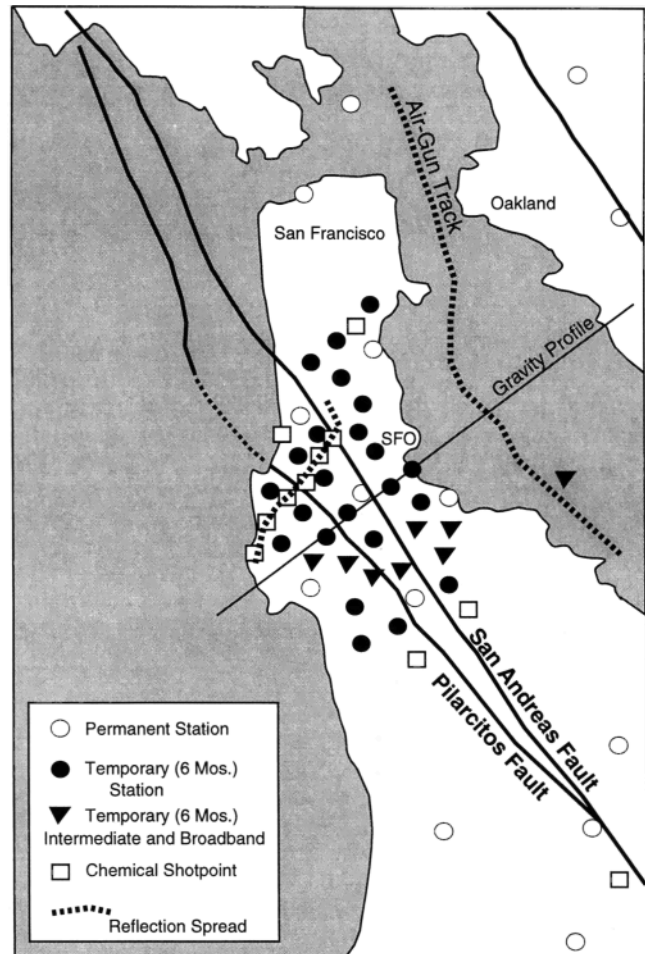
Figure 3. Setup and location of the 1995 San Francisco Peninsula seismic experiment. Locations of our temporary network (solid circles and triangles) and permanent Northern California Seismic Network (NCSN) stations (open circles) are shown. The dashed line in San Francisco Bay marks the approximate track line for air gun shots recorded by the network. Squares show the locations of chemical explosive shot points, and the dashed line on the Peninsula shows the location of the high-resolution refraction spread.
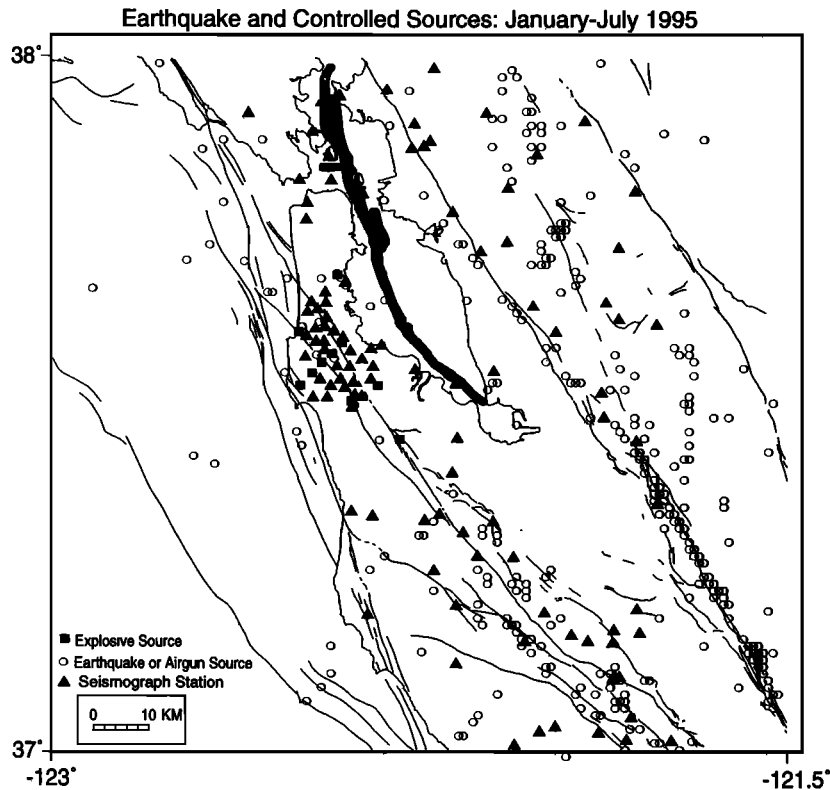
Figure 4. Relocated epicenters of the earthquake sources (January–July 1995) and locations of the controlled sources (open circles) used in our travel time inversion for 3-D velocity structure of San Francisco Peninsula. Our temporary network and the NCSN stations used for the regional velocity model are shown as solid triangles.

Travel Time Inversion for 3-D Upper Crustal Velocity Structure of San Francisco Peninsula

Travel Time Data

Four separate types of travel time data were applied to our velocity modeling: (1) first-arrival times from local earthquakes (Figure 5), (2) first-arrival times from air gun blasts in San Francisco Bay (Figure 6), (3) first-arrival times from explosive sources detonated on San Francisco Peninsula (Figure 7), and (4) travel time picks from earthquake and controlled sources from the NCSN catalog and previous regional seismic experiments [*Murphy et al.*, 1992; *Brocher and Moses*, 1993; *McCarthy and Hart*, 1993; *Brocher and Pope*, 1994; *Kohler and Catchings*, 1994; *Holbrook et al.*, 1996]. We used NCSN origin times to window out the local earthquakes, sorted the data into receiver gathers, and plotted them as a function of offset to epicenters (for ease of picking; NCSN hypocentral locations were used as initial input for velocity modeling). Figure 5 shows an example of a quiet site; data quality was degraded in more urban sites where cultural noise overwhelmed some of the smaller events. Some of the apparent perturbations in arrival times shown in Figure 5 result from variable hypocentral depths of events that affected the lengths of the travel paths to the receiver and hence the arrival times. We picked the first arrival times (*Pg* phase) of all usable, well located (by the NCSN) earthquakes during the January–July 1995 period on the 31 instruments in our array (~180 events with an average of 105 recorded at a particular site). We applied the criteria that a well-located event was recorded by at least five permanent network stations and that the RMS error in location was less than 2 km. Only
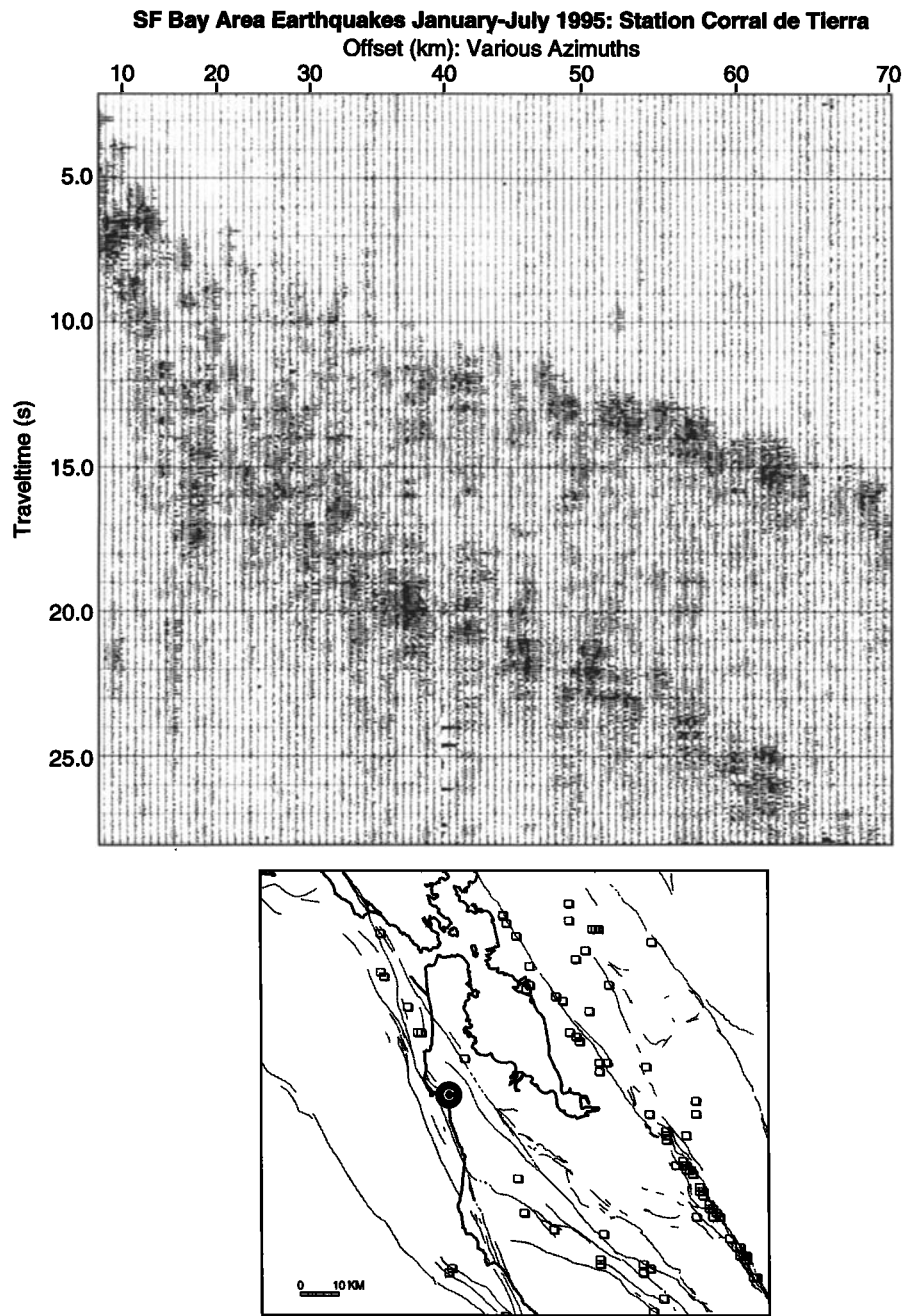
the smallest earthquakes ($<M$ 1.0) were near the limits of our criteria. Events were not picked if the onset of the *Pg* phase could not be confidently identified within 100 ms. We applied the same selection criteria to picks from the ~30-year NCSN catalog for use in the regional velocity model.

Airgun sources were detonated in San Francisco Bay in April 1995 over 9 days of shooting mostly along north-south profiles (Figure 4). Figure 6 shows an example of airgun data recorded at the same site as the earthquake data shown in Figure 5. The *Pg* phase from the air gun shooting was quite strong in most cases across our network. No clear secondary phases such as reflections were observed from the airgun data. Explosive source data are shown in Figure 7 from the same site as Figures 5 and 6. Clear first arrivals (*Pg* phase) were observed on all 31 of our stations from the explosive sources, though no coherent secondary phases were observed. We also included traveltime picks provided by investigators of previous controlled source experiments in the San Francisco Bay area in the regional velocity model [*Murphy et al.*, 1992; *Brocher and Moses*, 1993; *McCarthy and Hart*, 1993; *Brocher and Pope*, 1994; *Kohler and Catchings*, 1994; *Holbrook et al.*, 1996].

Velocity Modeling Methods

We applied the 3-D tomographic technique of *Hole* [1992] modified to simultaneously invert for velocity, hypocenters, and origin times. This technique applies a finite difference solution to the eikonal equation (*Vidale* [1990]; updated by *Hole and Zelt* [1995]) to calculate first arrival times through a gridded slowness model. An iterative nonlinear inversion is performed as a simple backprojection along raypaths deter-

SF Bay Area Earthquakes January-July 1995: Station Corral de Tierra
Offset (km): Various Azimuths

Figure 5. Example plot of network earthquake data recorded at station Corral de Tierra (marked as C on the map); earthquake epicenters are shown as open squares on the map. Very clear first arrivals (Pg phase) are seen, as well as the direct shear wave arrivals (Sg phase) below. The data are plotted as a function of offset independent of azimuth or hypocentral depth. The arrival times were picked as a function of hypocentral location as determined by the NCSN for use in the velocity modeling. A 20-s automatic gain control (AGC) window was used for the display.

mined from the forward modeling step. We compiled travel-time picks from a variety of data types for each receiver as a function of their 3-D spatial source locations and inverted them for 3-D velocity structure. Initial hypocenter locations and origin times of earthquakes were input as determined by the NCSN. Starting models were discretized into grids of 1-km cells; we used small grid cells to ensure accurate calculation of ray paths along short source-receiver offsets. A spatial smoothing filter was applied to the models between velocity and source-parameter iterations. Early iterations were conducted

that tested a variety of 1-D starting models, applied very broad smoothing filters (up to 100 km), and limited source-receiver offset ranges to solve the shallowest parts of the velocity model first. Subsequent iterations were conducted that included greater source-receiver offsets and progressively shorter smoothing filters.

The San Francisco Bay area is crossed by several major strike-slip faults that provided most of the seismicity we used to develop the velocity models presented here. These strike-slip faults also cause heterogeneous velocity structure in the seis-

mogenic crust. The earthquakes used in this study were initially located with a 1-D velocity model; thus a degree of coupling between hypocenter location and the velocity structure derived from earthquake travel times is unavoidable and could cause significant errors in the resolved velocity models [e.g., *Thurber*, 1993]. To reduce such errors, hypocenters and origin times were relocated while controlled source locations and times were held fixed. The events were relocated between velocity iterations (mean relocation was 0.54 km); see J. A. Hole et al. (Seismic tomography in the San Francisco Bay area, submitted to *Journal of Geophysical Research*, 1996; hereinafter referred to as Hole et al., submitted manuscript, 1996) and *Hole* [1992] for full details on the travel time inversion algorithm.

We found it necessary to model 3-D velocity structures on two separate scales so that we could use regional earthquake sources recorded by our local network: (1) a San Francisco Bay regional model, and (2) a local San Francisco Peninsula model. The regional-scale model was developed by applying the ~30-year catalog of NCSN first-arrival travel time picks and picks from previous controlled source experiments to generate a velocity solution that included the entire San Francisco Bay region earthquake source areas (Plate 1). This model converged to an RMS travel time misfit of 370 ms after 7 iterations. A 10-km smoothing filter was applied to the final regional model, which was masked in areas of no ray coverage for display (Plate 1). A complete interpretation of San Francisco Bay regional velocity models is provided by Hole et al. (submitted manuscript, 1996).

The purpose for generating the San Francisco Bay regional velocity model was to enable travel times from earthquake sources located outside our San Francisco Peninsula network to be calculated to the edges of a second, more detailed model (our 1-3 km spaced network allowed for a much shorter smoothing filter than did the 5-20 km spaced NCSN). Thus in effect, the distant earthquake sources were migrated to the edges of a more detailed model and treated like deep sources along the model faces; this technique somewhat resembles a teleseismic experiment in that traveltime variations from distant sources were used to augment a local array study. The uncertainties in source location and travel time misfits of the regional model may accumulate on long travel paths and could cause errors in the travel time calculations to the edges of the more detailed model. In practice, however, such uncertainties manifested primarily as small static velocity shifts at depth in the resolution tests. The application of controlled sources from known locations acted to calibrate the velocity models. In combination with fixed sources, short smoothing parameters (2 km) and the close station spacing (1-3 km) prevented significant spatial shifting of velocity anomalies. Intentional static mislocation of earthquake sources in test models caused very minor changes in resolved velocity; these effects are quantified in a subsequent discussion.

The 3-D Velocity Structure of San Francisco Peninsula

A 3-D velocity model limited to San Francisco Peninsula was developed by shortening the final smoothing filter to 2 km in accordance with the 1-3 km station spacing adopted for the temporary network. The San Francisco Peninsula model converged to an RMS traveltime misfit of 245 ms after 5 iterations. Like the San Francisco Bay regional velocity model, the San Francisco Peninsula velocity model was masked in areas of no ray coverage (Plate 2 and Figure 8). Plate 2 shows horizontal slices (20 km × 20 km) taken from the 3-D model volume; the

shallowest slice (1 km depth) shows a velocity range from ~3.5 to 5.0 km/s. A very rough correspondence of velocity to the trace of the present-day San Andreas fault is evident, with higher velocities occurring on the southwest side of the fault trace; this velocity boundary near the San Andreas fault is more clearly shown in the vertical cross section of Plate 3. The shallow velocity structures resolved at 1-km depth correlate broadly with mapped geologic units; the higher velocity rocks (4.5-5.0 km/s) southwest of the San Andreas correlate with Franciscan sandstones and greenstones (metamorphosed oceanic basalts) of the Permanente terrane, the intermediate velocity rocks (4.0 km/s) immediately northeast of the San Andreas correlate with highly sheared Franciscan rocks, and the lowest velocity rocks (3.5 km/s) correlate with Quaternary and Tertiary basin fill [*Brabb and Pampeyan*, 1983]. The maximum error in reported velocities at specific points is ±0.4 km/s (±0.2 km/s if averaged over a 2-km-wide zone) as determined from resolution tests (discussed in a subsequent section). There are indications of some lower-velocity rocks within the Permanente terrane just northeast of the Pilarcitos fault; these rocks are investigated in detail in a higher-resolution two-dimensional (2-D) model shown in Figure 11.

At 3 km depth the highest velocity rocks (5.5 km/s) appear to be confined between the downward vertical projection of the surface traces of the San Andreas and Pilarcitos faults, and probably represent the deeper expression of the Franciscan greenstones mapped at the surface, or a higher velocity unit underlying the Permanente terrane. Southwest of the Pilarcitos fault is a large outcrop of Cretaceous granite (Montara Mountain Granite) that is part of the Salinian block [*Brabb and Pampeyan*, 1983]. Although velocities within the Salinian block are higher in general than the Franciscan rocks juxtaposed across the San Andreas fault to the east (Plate 1), beneath the upper 1 km on San Francisco Peninsula, Franciscan greenstone rocks are often higher velocity than the Salinian Montara Mountain Granite (Plate 2). As will be shown, modeling of higher resolution refraction data indicates that the Montara Mountain Granite is faster than the Permanente terrane in the uppermost 1 km (Plate 4).

Below 3-5 km depth it appears that a downward vertical projection of the surface trace of the Pilarcitos fault marks a velocity transition from lower velocities to the southwest (5.5-6.0 km/s) into higher velocities to the northeast (6.2-6.8 km/s) (especially evident at 7 km depth, Plate 2). Our resolution tests indicate that beneath 6 km depth, velocity anomalies can only be resolved within about 2 km of their true positions. Thus this lateral velocity change could reasonably be attributed to either the San Andreas or Pilarcitos faults. At 7 km depth, there is a small (~5 km × 5 km) high velocity anomaly (6.5-6.8 km/s) just northeast of the San Andreas fault (see contours on Plate 2). This body lies at the western edge of a larger high-velocity anomaly (~6.2 km/s) that lies beneath much of San Francisco Bay at ~6-7 km depth that appears to be bounded by the Hayward fault on its east side (Plate 1). The small 6.5-6.8 km/s anomaly may represent a high-velocity unit within the Franciscan Complex that has velocities appropriate for diabase or diorite lithologies at 5-10 km depths [e.g., *Christensen and Mooney*, 1995]. These high velocities are not typical of Franciscan rocks at shallow depths; the regional average is lower at 6.0-6.2 km/s [e.g., *Holbrook et al.*, 1996]. If the ±0.2 km/s limit on absolute velocity resolution is taken into account, then the 6.5-6.8 km/s rocks could still fall into the average range for Franciscan rocks. Beneath 7 km depth, there are hints of struc-
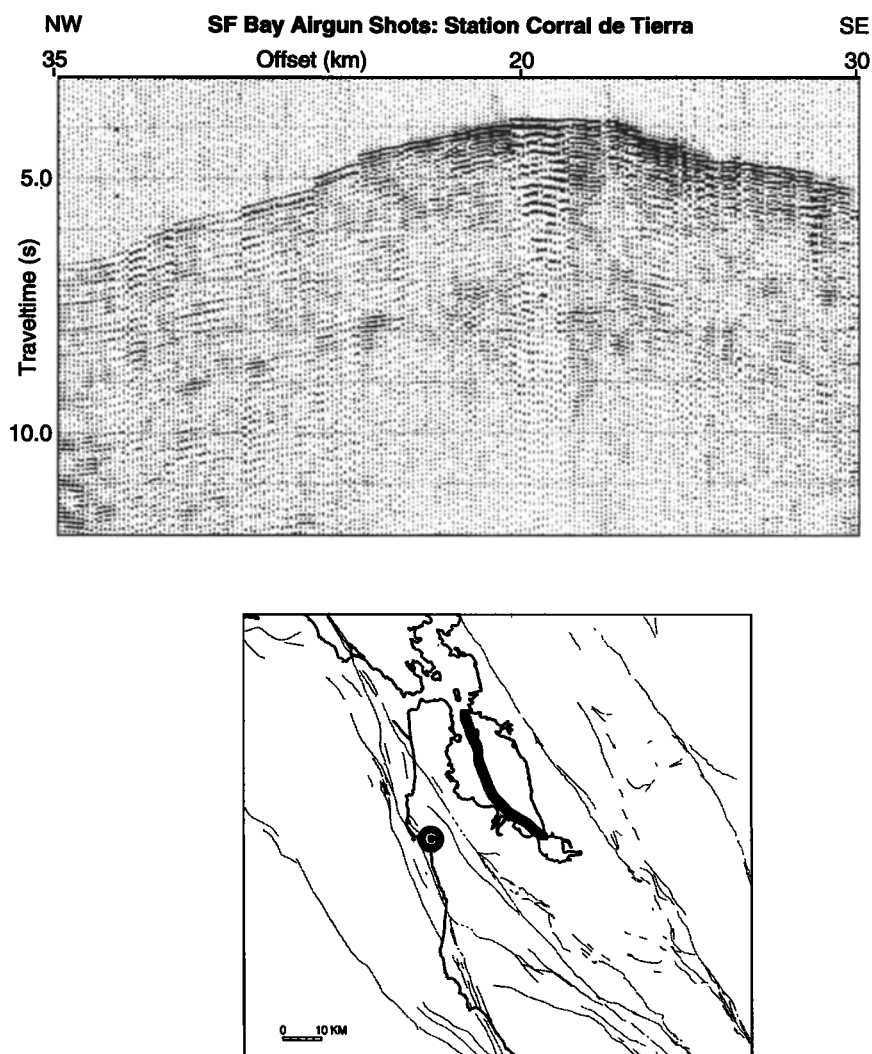
Figure 6. Example data plot from one line of air gun shots recorded at station Corral de Tierra (marked as C on the map). Air gun shots were also recorded from northern San Francisco Bay (Figure 4). Clear Pg arrivals can be seen, but no secondary arrivals such as reflections were recorded from air gun sources by the network. The apparent time skips in the first arrivals result from gaps in the shooting; the data are plotted in trace order to enable clearer examination. A 5-s AGC window was used for the display.

tures that could be bounded by downward vertical projections of the Pilarcitos and San Andreas faults, but there is limited coverage at these depths and such correlations are tentative. More typical Franciscan velocities of ~6.0–6.2 km/s are observed at these depths.

An implication of the San Francisco Peninsula 3-D velocity model is that at 3 km, and perhaps extending to 7 km depth, there are velocity boundaries that can be correlated to the downward vertical projection of the Pilarcitos fault (Plate 2). Such a correlation suggests that the Pilarcitos fault may be a high-angle feature. High-angle velocity changes are also evident across the San Andreas fault and are strongest in the shallowest part of the upper crust (1–3 km) where there is an apparent high-angle boundary between the Franciscan Permanente terrane southwest of the fault and highly sheared Franciscan rocks to the northeast (Plates 2 and 3). In Plate 3, we show a representative vertical southwest-northeast oriented slice through the 3-D model volume. Because most of the structural variation occurs from southwest to northeast (perpendicular to the major faults), vertical velocity sections

through the model are very similar from north to south. The primary feature in these slices is a consistent gradation from higher-velocity rocks southwest of the San Andreas fault into lower-velocity rocks northeast of the fault in the upper 3 km of the crust.

Dip of the Pilarcitos Fault

We conducted a higher-resolution 2-D travel time inversion for the velocity of the Permanente terrane (bounded along its southwest side by the Pilarcitos fault) using travel times recorded on instruments (SGRs) along a closely spaced (50-m station spacing, 2–3 km shot spacing) southwest-northeast directed recording spread (Figure 3 and Plate 4). The spread was oriented at a ~90° angle to the strikes of the Pilarcitos and San Andreas faults. Because of the short station spacing and overlapping coverage we were able to reduce the velocity model cell size to 100-m squares (as compared with the 1-km cubes in the 3-D velocity models). Models derived from the 2-D higher-resolution refraction data are most consistent with the Pilarcitos fault marking a vertical boundary in the upper 0.5–1.0 km
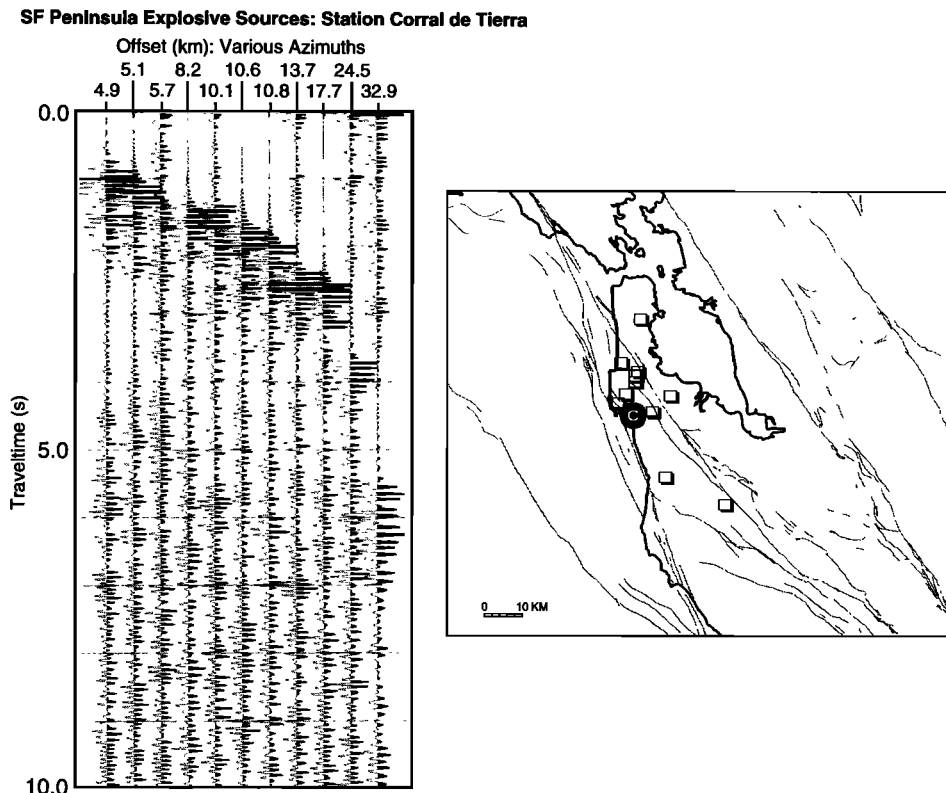
Figure 7. Example plot of explosive-source data recorded at station Corral de Tierra (marked as C on the map). Clear *Pg* arrivals can be seen, but no secondary arrivals such as reflections were recorded from explosive sources by the network. Locations of the explosive sources are shown as open squares on the inset map. A 5-s AGC window was used for the display.

of the crust between the relative low-velocity rocks of the Permanente terrane to the northeast (~4.5 km/s) and the adjacent Salinian rocks to the southwest (Plate 4). The higher-resolution results tend to verify the indications from horizontal slices out of the 3-D velocity model (Plate 2) that the Pilarcitos fault is a steeply dipping boundary. We thus interpret the Pilarcitos fault as primarily a strike-slip fault rather than a thrust. We discuss the tectonic implications of the Pilarcitos fault as a transform in a subsequent section.
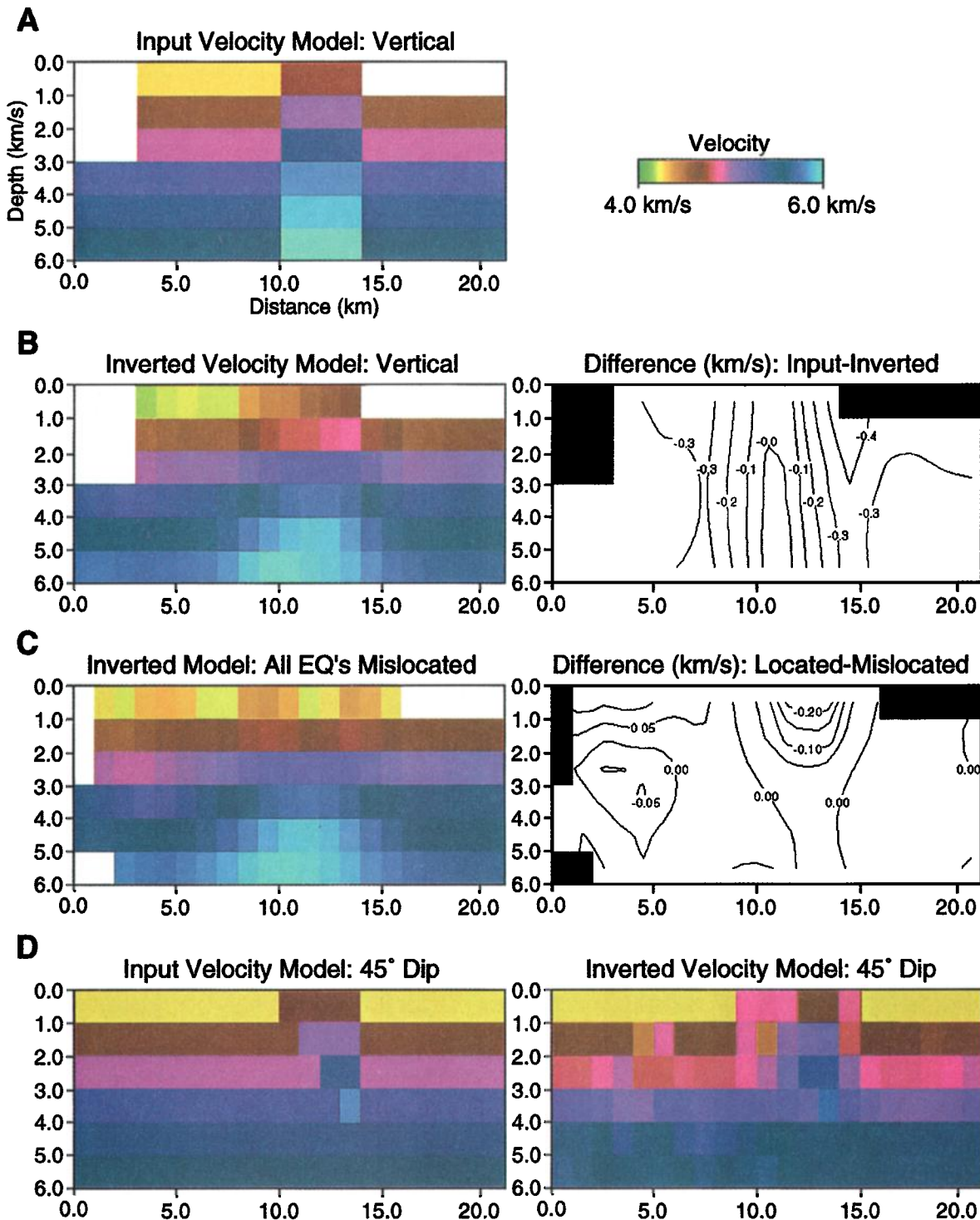
Resolution

To interpret results from tomographic inversions for velocity structure, it is very important to quantify what features are resolvable given the quantity and coverage of the input travel time data. We conducted a number of resolution tests like the examples shown in Plate 5; 3-D test models were constructed with velocity anomalies superimposed on 1-D gradients, and groups of synthetic travel time picks were calculated from all the source locations into the station locations used in the actual modeling. These synthetic travel time picks were then inverted for velocity structure following the same procedures used to model the real data (1-D starting models; 2-km smoothing filter in final iterations), and the final models were compared with the test models to see how well they could be reproduced. We show the results of these example resolution tests as vertical slices to make it easier to evaluate changes in resolution with depth. In the examples shown in Plates 5a–5c, a 4-km-wide higher-velocity block (anomaly gradient increasing with depth a laterally consistent 0.5 km/s greater than the

background gradient) was superimposed beneath San Francisco Peninsula to mimic vertical structures. In addition, we conducted similar tests with dipping boundaries in an effort to ensure that we had sufficient coverage to discern moderately dipping (45°) velocity boundaries from vertical boundaries (Plate 5d).

Because the solution of velocity anomaly position and absolute velocity are coupled, there are trade-offs between resolving the shapes and positions of anomalies and their velocities. If we applied a strict criterion of absolute velocity resolution at specific points, we would find that the minimum reliably detectable velocity contrasts were 0.5 km/s (for the 3-D model data coverage). If instead, we allowed for smearing of anomaly positions, we could resolve smaller velocity contrasts (0.2–0.25 km/s). In addition, as might be expected, lateral resolution decreases with increasing depth because the Fresnel zone width of turning rays becomes increasingly broader. For example, in the 3-D model resolution tests, the lateral positions of vertical velocity contrasts (≥0.5 km/s) were resolvable to within 1 km of their actual positions near the surface, while at 5–6 km depth the boundaries can be smeared across 2-km-wide zones. Thus a fault or other velocity interface that is vertical might appear to dip anywhere between 70° and 110°. Similarly, a 70°–110° dipping interface could appear vertical. In Plate 5b we contoured the difference between the actual velocities and the modeled velocities of a representative resolution test to demonstrate the magnitudes of errors; we found that the centers of the input velocity anomalies (≥0.5 km/s) tended to be resolved exactly, while the blurred edges of the
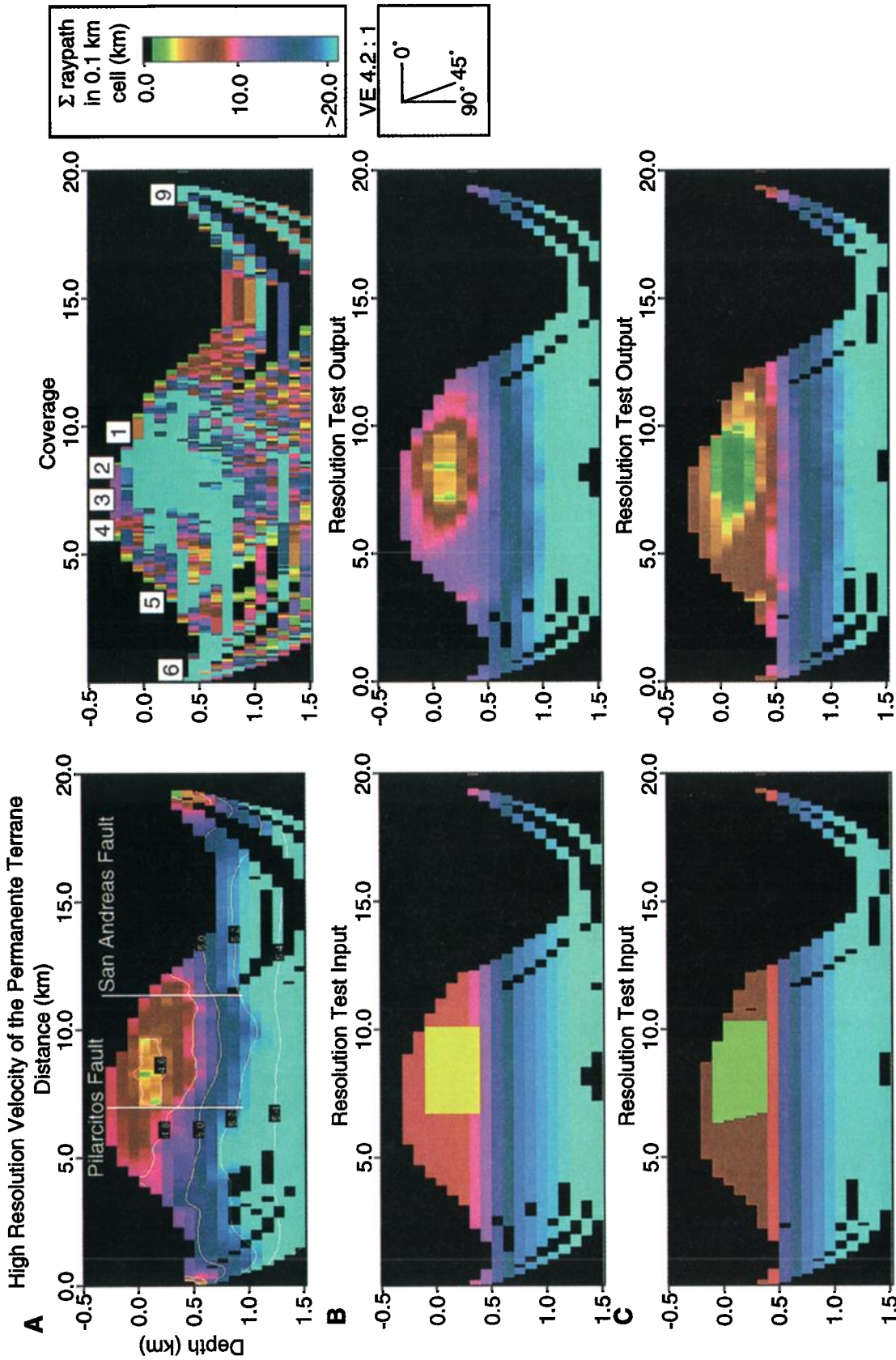
Plate 4. Two-dimensional high-resolution velocity model of the Permanente terrane between the Pilarcitos and San Andreas faults created using first breaks from seismic reflections data (location shown in Figure 3). (a) An apparent steeply dipping to vertical velocity boundary was resolved that corresponds with the Pilarcitos fault in the upper 0.5–1.0 km of the crust. (b) Resolution test for a vertically bounded low-velocity anomaly; synthetic travel time picks were generated with the model on the left and were inverted for the model on the right using the actual station and shot locations. (c) Resolution test for a 45° east dipping boundary on a low-velocity anomaly. Lateral smearing of the boundary causes the modeled result to underestimate the dip on the anomaly.

A

Input Velocity Model: Vertical

Velocity

4.0 km/s   6.0 km/s

B

Inverted Velocity Model: Vertical

Difference (km/s): Input-Inverted

C

Inverted Model: All EQ's Mislocated

Difference (km/s): Located-Mislocated

D

Input Velocity Model: 45° Dip

Inverted Velocity Model: 45° Dip

Plate 5. Example resolution tests. (a) A simple vertical high-velocity zone (0.5 km/s faster on same gradient as background) was emplaced in a 1-D velocity gradient. Travel times were calculated through this test model from source locations used in the San Francisco Peninsula velocity model to the network station locations to generate synthetic travel time picks. (b) The synthetic travel time picks were then inverted for velocity, and the resulting model is shown along with contours of the difference between the input velocities and modeled velocities. The boundaries of the input velocity anomaly were blurred (1–2 km, especially at the bottom of the model). The absolute velocities were resolved completely at the center of the anomaly but differ by as much as 0.4 km/s at the edges; the average mismatch across a 2-km-wide zone at the anomaly edge was 0.2 km/s. (c) All earthquake sources were intentionally mislocated (by 2 km in random directions) to investigate the effects of mislocated sources. The controlled sources were kept fixed. The position of the velocity anomaly was not shifted as a result of source mislocation, but static velocity shifts (up to 0.2 km/s) were observed. Systematic mislocations produced similar results as random mislocations. (d) Resolution test similar to vertical example above, but with a 45° dipping interface. Coverage was sufficient to resolve a dipping boundary in the upper 4 km of the model.
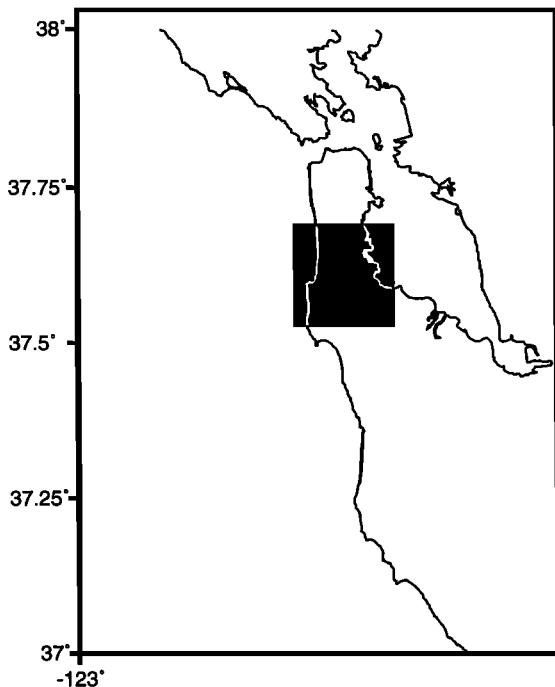
Figure 8. Location map showing the boundaries of the horizontal slices shown in Plate 2.

anomalies had worst-case velocity mismatches of up to 0.4 km/s. If the velocity mismatches are averaged across the 2-km-wide blurred edge of the output velocity model, then velocity resolution is 0.2 km/s.

We conducted similar resolution tests for the higher resolution 2-D model (Plate 4). We found that we could resolve a test rectangular low-velocity anomaly (anomaly gradient increasing with depth a laterally consistent 0.3 km/s less than the background gradient) within 100 m of its actual vertical and horizontal position and to within 0.1 km/s in velocity. We tested vertical and dipping (45°) velocity boundaries and found that a 45° dipping boundary was easily resolvable despite the lateral smearing effect that tended to overestimate the amount of dip on the boundary (Plate 4).

In addition to spatial and velocity resolution tests, we attempted to isolate errors resulting from mislocation of earthquake hypocenters; the RMS travel time misfit (370 ms) of the regional velocity model resulted from mislocated hypocenters, broad smoothing filters, and picking errors. Simultaneous inversion for hypocenters, origin time, and velocity reduced errors caused by the 1-D velocity model applied for NCSN hypocenter locations, but it is still worthwhile to investigate effects of possible earthquake mislocation because the 10-km smoothing filter applied to the regional model most likely preserved some of the coupling between velocities in the source zones and the source/time locations. To gain some insight on the effects of source location errors, we intentionally mislocated the earthquake sources in our resolution tests. To investigate a worst-case effect of mislocated events, we systematically (and randomly) moved all earthquakes by the maximum RMS mislocation error (from 1-D velocity model used for NCSN locations) of events included in our modeling (2 km) while keeping the controlled sources fixed. In Plate 5c, we show the effects of source location errors on the geometry and magnitude of velocity anomalies; the effects of mislocating all

earthquake events on the modeled velocity structure were minor. The locations of the velocity boundaries did not have to be shifted laterally, though small static differences in the velocity magnitudes were observed (0.2 km/s; this number is a maximum estimate because the source error estimates assumed maximum RMS mislocations and no correction from hypocenter relocation) (Plate 5c). The lack of large lateral velocity anomaly shifts occurred primarily because the travel paths of first arrivals from distant earthquake sources were mostly high angle. Similar results occurred with random mislocations as with systematic mislocations; the static velocity shifts were very slightly different, probably a result of net cancellation of location errors. We conclude from our resolution tests that in the upper 6 km of the San Francisco Peninsula crust, we can resolve the dip on lateral velocity boundaries to within ±20°, and absolute velocities to within ±0.2 km/s across a 2-km-wide zone.

A 2-D Gravity Model Across San Francisco Peninsula

Our interpretation of the anomalies from the San Francisco Peninsula velocity models is that the velocity boundaries associated with both the Pilarcitos and San Andreas faults are steeply dipping to vertical features (70°–110°). Such an interpretation is consistent with gravity data on the northern Peninsula (shown above the modeled cross section on Figure 9) that indicate a dense block located between the San Andreas and Pilarcitos faults. This dense block coincides with the Franciscan Permanente terrane oceanic rocks, which are denser than other units within the Salinian and Franciscan terranes. There is an associated relative velocity increase of the Permanente terrane in the shallow crust (0–5 km depth; Plate 2). Our 2-D cross-section gravity model (Figure 9) indicates that the Permanente terrane is ~0.055 g/cm^3 denser than the Salinian block and 0.085 g/cm^3 denser than the Franciscan rocks northeast of the San Andreas fault (we model only a small density contrast (0.03 g/cm^3) between the Salinian block and non-Permanente Franciscan rocks). All densities used in the modeling are consistent with the range of measured values in a database of rock densities in the Bay Area [*Jachens and Griscom*, 1997].

The gravity data are not consistent with a thrust fault geometry for the Pilarcitos. Curve a on Figure 9 is the predicted gravity signature for a 45° NE dipping Pilarcitos fault that merges at depth with a vertical San Andreas fault. This geometry produces a small (~2 mGal) local high directly over the Permanente rocks between the two faults but fails to explain the longer-wavelength high centered on the Pilarcitos and San Andreas faults because of the low-density contrast between the Salinian and Franciscan to the east which would be juxtaposed across the San Andreas at depth beneath a Pilarcitos "thrust." Because of the nonuniqueness of gravity modeling, the northeastern limb of the long wavelength high could be replicated for a Pilarcitos "thrust" interpretation if the density contrast of the Salinian block was increased relative to Franciscan rocks from 0.03 to 0.05 g/cm^3; however, this results in gravity values significantly larger than observed over the Salinian block (see curve b on Figure 9). Modeling of a detailed gravity profile 15 km to the southeast also indicates near vertical boundaries associated with the San Andreas and Pilarcitos faults, a substantially dipping "thrust" geometry for the Pilarcitos fault (~45°NE) can be excluded by these data (R. Jachens, written
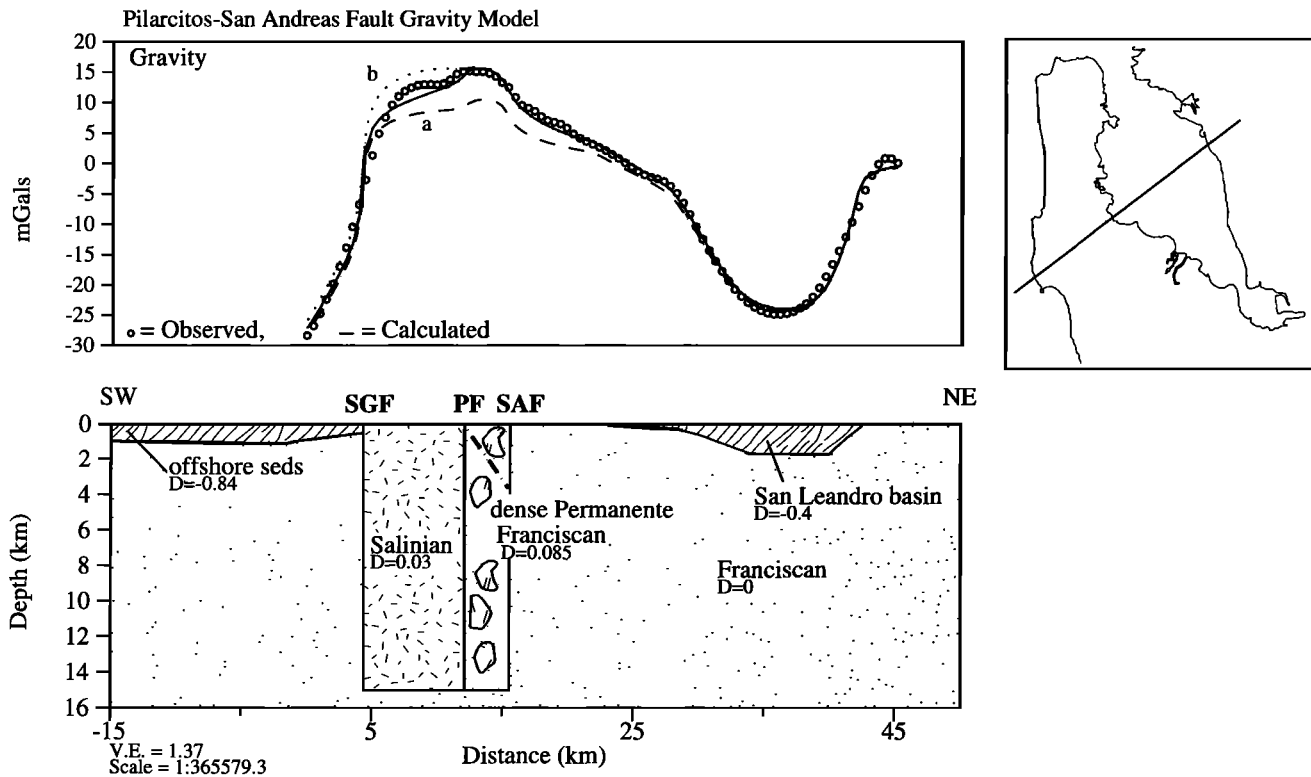
Figure 9. Two-dimensional gravity model across the San Francisco Peninsula; locations of the San Andreas (SAF), Pilarcitos (PF), and San Gregorio (SGF) faults are indicated, and density contrasts (D) are given in grams per cubic centimeters. The best fit (solid curve) to the Bouguer anomaly was with vertical density boundaries across both the San Andreas and Pilarcitos faults. The fit for a 45°NE dipping geometry for the Pilarcitos fault (indicated by heavy dashed line on cross section) is given by dashed curve a. The fit for the same dipping model but with an increased density (to 0.05 g/cm³) in the Salinian block is given by dotted curve b. The irregular bodies within the Permanente terrane do not contribute as density bodies; they are meant to symbolize fragments of oceanic crust.

communication, 1995). Thus, while nonunique, the Bouguer gravity data interpretation as constrained by measured density values appears generally consistent with a steep fault interpretation for both the San Andreas and Pilarcitos faults. A high-angle interpretation of the Pilarcitos fault combined with geologic evidence such as the presence of Salinian rocks west but not east of the Pilarcitos fault and the 19–23 km offset limit of the Franciscan Permanente terrane along the Peninsula segment of the San Andreas fault support the idea that the Pilarcitos fault accommodated most of the pre-Quaternary right-lateral plate boundary slip on San Francisco Peninsula.
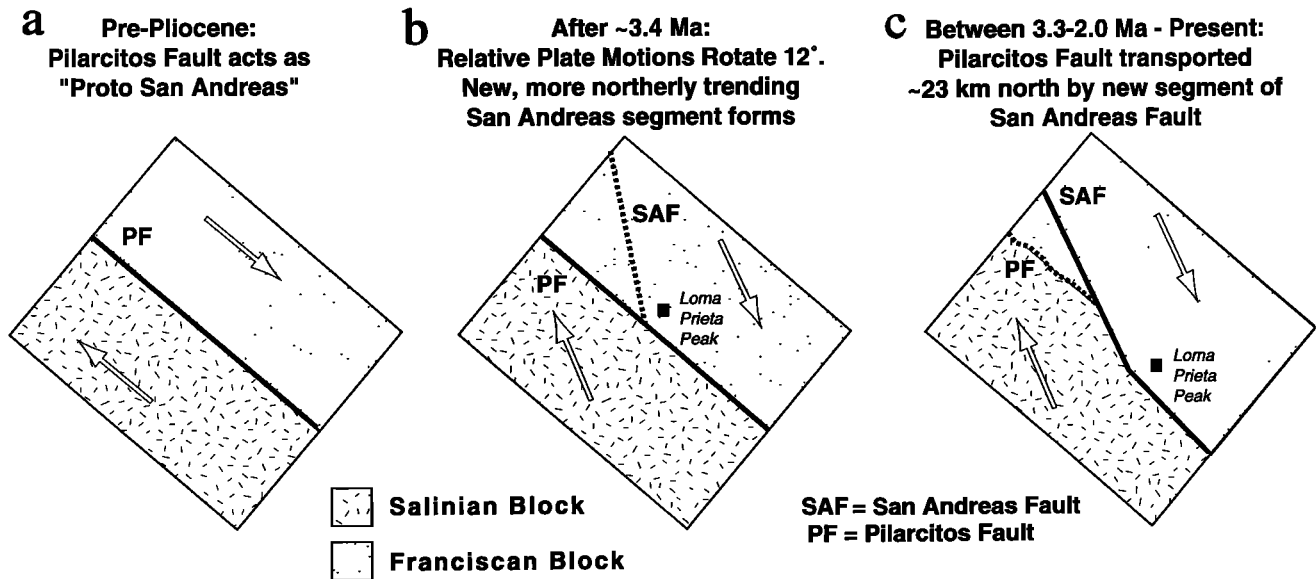
Upper Crustal Faulting Interpretation and Tectonic Implications

If our interpretation of the anomalies from the San Francisco Peninsula velocity and gravity models is accepted that the Pilarcitos and San Andreas faults are steeply dipping to vertical features (70°–110°), then there are important tectonic implications for the recent geologic history of San Francisco Peninsula. We suggest a simple model for the evolution of plate boundary faulting on the Peninsula that resulted from an apparent 11°–12° clockwise change in convergence angle between the Pacific and North American plates about 3.4–3.9 Ma [*Harbert and Cox*, 1989; *Harbert*, 1991]. In that model, the ~N45°–50°W striking Pilarcitos fault would have been well-oriented to accommodate Pacific-North American plate motions prior to

3.4–3.9 Ma. When the relative motion changed to the present N32°–33°W direction on the peninsula, the resulting component of convergence made slip on the Pilarcitos fault more difficult, eventually resulting in the formation of a new, more favorably oriented fault strand, the N30–35°W striking peninsula segment of the San Andreas fault (Figure 10). Similar changes in fault trends or formation of new faults apparently occurred throughout coastal California during the 3.4–3.9 Ma period [*Harbert and Cox*, 1989; *Harbert*, 1991].

The initiation of the peninsula segment of the San Andreas fault can be estimated from the geologically determined 19–23 km offset of the Permanente terrane along the San Andreas fault and the averaged long-term slip rate. As noted in the introduction, geodetic data [*Lisowski et al.*, 1991; *Williams*, 1995] and late Holocene slip rate studies [*Hall*, 1984, 1993; *Hall et al.*, 1996] have suggested a present-day slip rate of 15–17 mm/yr on the peninsula segment of the San Andreas fault, whereas studies based on longer-term geologic data have suggested a lower rate of 7–12 mm/yr [*Cummings*, 1968; *Taylor et al.*, 1980]. The lower slip rate estimates are probably more representative of the true averaged long-term slip rate since there was no doubt some delay before the newly formed peninsula segment of the San Andreas fault (with an initial slip rate of 0 mm/yr) was able to achieve the present day 15–17 mm/yr rate. Using the geologic slip rate of 7–12 mm/yr, the ~23 km best estimate offset [e.g., *Dibblee*, 1966; *Cummings*,

a **Pre-Pliocene:**
Pilarcitos Fault acts as
"Proto San Andreas"

b **After ~3.4 Ma:**
Relative Plate Motions Rotate 12°.
New, more northerly trending
San Andreas segment forms

c **Between 3.3-2.0 Ma - Present:**
Pilarcitos Fault transported
~23 km north by new segment of
San Andreas Fault

Salinian Block

Franciscan Block

SAF = San Andreas Fault
PF = Pilarcitos Fault

Figure 10. Model for the development of the San Andreas and Pilarcitos faults. (a) Before Pliocene time the Pilarcitos acted to accommodate most of the right-lateral strain on San Francisco Peninsula, offsetting the Franciscan and Salinian terranes. (b) About 3.4–3.9 Ma, the relative plate motion between the Pacific and North American plates changed resulting in an 11°–12° clockwise increase in the convergence direction, sometime afterward a new more northerly trending segment of the San Andreas fault system developed. (c) Sometime between 3.3 and 2.0 Ma, the Pilarcitos fault was abandoned and transported ~23 km northwest along the San Andreas fault.

1968; R. C. Jachens, personal communication, 1996] implies that the present-day Peninsula segment of the San Andreas fault originated sometime between 2.0 and 3.3 Ma. The older end of this time range is similar to the timing of the 11°–12° clockwise change in convergence angle between the Pacific and North American plates about 3.4–3.9 Ma [*Harbert and Cox*, 1989; *Harbert*, 1991].

The offset of the Calera limestone in the Permanente terrane implies that the Pilarcitos fault has been translated ~23 km northwestward; its reconstructed location lies northwest of Loma Prieta Peak in the central Santa Cruz Mountains within a broad bend in the San Andreas fault system (Figure 1). As shown in Figure 10, the Pilarcitos fault on San Francisco Peninsula was probably part of the present-day San Andreas fault system from the Loma Prieta area south. *McLaughlin et al.* [1991] and *McLaughlin and Clark* [1997] have mapped what they infer to be the main offset strand of the Pilarcitos fault in the Loma Prieta area (equivalent to the main "bedrock" component of the San Andreas fault based on a major difference in Pliocene and younger stratigraphy) just a few hundred meters northeast of the San Andreas fault where it ruptured during the 1906 San Francisco earthquake.

The N30°–35°W strike of the San Francisco Peninsula segment of the San Andreas fault is within 1°–2° of the NUVEL-1 relative plate motion velocity vector at this latitude [*De Mets et al.*, 1990]; this strike is more northerly than the ~N45°W strike of the Pilarcitos fault on the peninsula, as well as its presumed offset equivalent, the present-day San Andreas fault in the Santa Cruz Mountains (Figures 1 and 10). Thus the N30°–35°W strike of the peninsula segment of the San Andreas fault and its initiation between 2.0 and 3.3 Ma suggest that it developed to more favorably accommodate plate boundary shear in response to the change in relative motion between the Pacific and North American plates. Faults east of San Francisco Bay

such as the Hayward fault (Figure 1) have inferred slower slip rates after 5 Ma (relative to rates between 8 and 5 Ma), suggesting a transfer of strain westward to the San Andreas system between 5 and 3 Ma [*McLaughlin et al.*, 1996]. The implication of this is that since the peninsula segment of the San Andreas fault did not exist prior to about 3 Ma, the Pilarcitos fault probably accommodated most of the regional plate boundary strain between 5 and 3 Ma.

The abrupt topography of the recently uplifted (<3 Ma) Santa Cruz Mountains west of the San Andreas fault [e.g., *Page*, 1992] indicates that there has been significant fault-normal compression across the peninsula segment of the plate boundary. It is possible that during the early initiation of the Peninsula San Andreas fault, the Pilarcitos fault (and possibly other subparallel faults in the San Andreas system) accommodated both dextral slip and convergence as oblique high-angle thrust faults, similar to the 70° southwest dipping fault plane responsible for the 1989 Loma Prieta earthquake that had almost equal components of right lateral and reverse motion. Such late phase oblique slip may be responsible for the curved or scalloped surface trace of the Pilarcitos fault (Figures 2 and 3).

While the seismic hazards posed by the peninsula segment of the San Andreas fault are obvious, the rupture potential of the Pilarcitos fault is far less so. If the Pilarcitos fault is subvertical and has a low shear strength like the San Andreas fault [e.g., *Lachenbruch and Sass*, 1980; *Zoback et al.*, 1987; *Rice*, 1992; *Sleep and Blanpied*, 1992; *Bird and Kong*, 1994], then it could still pose a hazard as a strike-slip fault despite its more north-westerly trend relative to the San Andreas. If the Pilarcitos fault plane is strictly vertical throughout the upper crust, then it cannot accommodate any convergent strain. However, given the ±20° resolution on the dip of velocity anomalies in our model, we cannot rule out some capability of the Pilarcitos fault to move as an oblique reverse fault, similar to the Loma

Prieta fault plane. Such a high-angle oblique reverse plane would require high fluid pressure or some other mechanism to allow it to move [e.g., *Sibson*, 1985], similar to what has been proposed for the Loma Prieta source region based on electrical and seismic studies [e.g., *Eberhart-Philips et al.*, 1990; *Zoback and Beroza*, 1993; *Eberhart-Philips et al.*, 1995].

Conclusions

A detailed 3-D velocity model for San Francisco Peninsula was generated from earthquake and controlled sources. We conclude from seismic and gravity data collected on San Francisco Peninsula, that the San Andreas and Pilarcitos faults are high-angle to vertical features where resolvable in the upper crust. Geologic data suggest that most Quaternary strike-slip offset on the San Francisco Peninsula has occurred on the San Andreas fault rather than on the more northwesterly oriented Pilarcitos fault, but we cannot rule out the Pilarcitos fault's potential to accommodate some oblique convergent strain as a high-angle reverse fault, similar to the fault associated with the Loma Prieta earthquake. Prior to about 3 Ma, the Pilarcitos fault probably accommodated most of the plate boundary strain; a change in the relative Pacific-North American plate motions ~3.4–3.9 Ma stimulated the formation of the Peninsula segment of the San Andreas fault, and the Pilarcitos fault was abandoned as the primary plate boundary fault.

References

Addicott, W. A., Late Pliocene mollusks from San Francisco Peninsula, California, and their paleogeographic significance, *Proc. Calif. Acad. Sci., 4th Ser., 37*, 57–93, 1969.

Bird, P., and X. Kong, Computer simulations of California tectonics confirm very low strength of major faults, *Geol. Soc. Am. Bull., 106*, 159–174, 1994.

Blake, M. C., Jr., Franciscan geology of northern California, *Field Trip Guideb. 43*, 254 pp., Pac. Sect., Soc. of Econ. Paleontol. and Minerol., Los Angeles, Calif., 1984.

Brabb, E. E., and E. H. Pampeyan, Geologic map of San Mateo County, California, *U.S. Geol. Surv. Misc. Invest. Ser. Map, I-1257-A*, 1983.

Brocher, T. M., and M. J. Moses, Onshore-offshore wide-angle seismic recordings of the San Francisco Bay Area seismic imaging experi-

ment (BASIX): The five-day recorder data, *U.S. Geol. Surv. Open File Rep., 93-0276*, 1993.

Brocher, T. M., and D. C. Pope, Onshore-offshore wide-angle seismic recordings of the San Francisco Bay Area seismic imaging experiment (BASIX): Data from the Northern California Seismic Network, *U.S. Geol. Surv. Open File Rep., 94-0156*, 1994.

Christensen, N. I., and W. D. Mooney, Seismic velocity structure and composition of the continental crust: A global view, *J. Geophys. Res., 100*, 9761–9788, 1995.

Cummings, J. C., The Santa Clara Formation and possible post-Pliocene slip on the San Andreas fault in central California, in *Proceedings of the Conference on Geologic Problems of the San Andreas Fault System*, edited by W. R. Dickinson and A. Grantz, *Stanford Univ. Publ. Geol. Sci., 11*, 191–207, 1968.

De Mets, C., R. G. Gordon, D. F. Argus, and S. Stein, Current plate motions, *Geophys. J. Int., 101*, 425–478, 1990.

Dibblee, T. W., Jr., Evidence for cumulative slip on the San Andreas fault in central and northern California, edited by E. H. Bailey, *Bull. Calif. Div. Mines Geol., 190*, 375–384, 1966.

Eberhart-Phillips, D., V. F. Labson, W. D. Stanley, A. J. Michael, and B. D. Rodriguez, Preliminary velocity and resistivity models of the Loma Prieta earthquake region, *Geophys. Res. Lett., 17*, 1235–1238, 1990.

Eberhart-Phillips, D., W. D. Stanley, B. D. Rodriguez, and W. J. Lutter, Surface seismic and electrical methods to detect fluids related to faulting, *J. Geophys. Res., 100*, 12,919–12,936, 1995.

Foxall, W., A. Michelini, and T. V. McEvilly, Earthquake travel time tomography of the southern Santa Cruz Mountains: Control of fault rupture by lithological heterogeneity of the San Andreas Fault Zone, *J. Geophys. Res., 98*, 17,691–17,710, 1993.

Hall, N. T., Holocene history of the San Andreas fault between Crystal Strings Reservoir and San Andreas Dam, San Mateo County, *Bull. Seismol. Soc. Am., 74*, 281–299, 1984.

Hall, N. T., Paleoseismic investigations of the San Andreas Fault on the San Francisco Peninsula, California, Technical Report, 15 pp., U.S. Geol. Surv., Menlo Park, Calif., 1993.

Hall, N. T., Wright, R. H., Clahan, K. B., 1996, Paleoseismic investigations of the San Andreas fault on the San Francisco Peninsula, California, *USGS-NEHRP Final Tech. Rep., 14-08-0001-G2081*, 45 pp., 1996.

Harbert, W., Late Neogene relative motions of the Pacific and North American plates, *Tectonics, 10*, 1–15, 1991.

Harbert, W., and A. Cox, Late Neogene motion of the Pacific plate, *J. Geophys. Res., 94*, 3052–3064, 1989.

Hart, P. E., J. McCarthy, and J. R. Childs, Deep seismic reflection profiling in San Francisco Bay: Results from the 1995 BASIX Bay Cable project (abstract), *Eos Trans. AGU, 76*(46), F398, 1995.

Hengesh, J. V., and J. Wakabayashi, Dextral translation and progressive emergence of the Pleistocene Merced basin and implications for timing of initiation of the San Francisco Peninsula segment of the San Andreas fault, in *Recent Geologic Studies in the San Francisco Bay Area, Publ. 76*, edited by E. M. Sangines, D. W. Anderson, and A. B. Buising, pp. 47–54, Pac. Sect., Soc. of Econ. Paleontol. and Mineral., Los Angeles, Calif., 1995.

Holbrook, W. S., T. M. Brocher, U. S. ten Brink, and J. A. Hole, Crustal structure of a transform plate boundary: San Francisco Bay and the central California continental margin, *J. Geophys. Res., 101*, 22,311–22,334, 1996.

Hole, J. A., Nonlinear high-resolution three-dimensional seismic travel time tomography, *J. Geophys. Res., 97*, 6553–6562, 1992.

Hole, J. A., and B. C. Zelt, 3-D finite-difference reflection traveltimes, *Geophys. J. Int., 121*, 427–434, 1995.

Jachens, R. C., and A. Griscom, Geologic and geophysical setting of the 1989 Loma Prieta earthquake, California, inferred from magnetic and gravity anomalies, *U.S. Geol. Surv. Prof. Pap., 1550*, in press, 1997.

Kelson, K. I., W. R. Lettis, and M. Lisowski, Distribution of geologic slip and creep along faults in the San Francisco Bay region, in *Proceedings on the Second Conference on Earthquake Hazards in the eastern San Francisco Bay Area*, edited by G. Borchardt, *Spec. Publ. Calif. Div. Mines Geol., 113*, 31–38, 1992.

Kohler, W. M., and R. D. Catchings, Data report for the 1993 seismic refraction experiment in the San Francisco Bay Area, California, *U.S. Geol. Surv. Open File Rep., 94-0241*, 1994.

Lachenbruch, A. H., and J. H. Sass, Heat flow and energetics of the San Andreas fault zone, *J. Geophys. Res., 85*, 6185–6222, 1980.

Lisowski, M., J. C. Savage, and W. H. Prescott, The velocity field along the San Andreas fault in central and southern California, *J. Geophys. Res.*, *96*, 8369–8389, 1991.

McCarthy, J., and P. Hart, Data report for the 1991 Bay Area seismic imaging experiment (BASIX), *U.S. Geol. Surv. Open File Rep.*, *93-0301*, 1993.

McLaughlin, R. J., and J. C. Clark, Geologic setting of the October 17, 1989 Loma Prieta earthquake, *U.S. Geol. Surv. Prof., Pap.*, *1550-A*, in press, 1997.

McLaughlin, R. J., J. C. Clark, E. E. Brabb, and E. J. Helley, Geologic map and structure sections of the Los Gatos 7 1/2′ Quadrangle, Santa Clara and Santa Cruz Counties, California, *U.S. Geol. Surv. Open File Rep.*, *91-593*, 1991.

McLaughlin, R. J., W. V. Sliter, D. H. Sorg, P. C. Russell, and A. M. Sarna-Wojcicki, Large-scale right-slip displacement on the East San Francisco Bay Region fault system, California: Implications for location of late Miocene to Pliocene Pacific plate boundary, *Tectonics*, *15*, 1–18, 1996.

Murphy, J. M., R. D. Catchings, W. M. Kohler, G. S. Fuis, and D. Eberhart-Phillips, Data report for 1991 active-source seismic profiles in the San Francisco Bay Area, California, *U.S. Geol. Surv. Open File Rep.*, *92-570*, 1992.

Olson, J., and G. A. Lindh, Seismicity of the San Andreas Fault from Cienega Winery to the Golden Gate, in *Minutes of the National Earthquake Prediction Evaluation Council, July 26–27, 1985, Menlo Park, California*, edited by C. F. Shearer, *U.S. Geol. Surv. Open File Rep.*, *85-0754*, 316–324, 1985.

Olson, J. A., and M. L. Zoback, Seismic deformation patterns on the San Francisco Peninsula, *Eos Trans. AGU*, *73*(43), Fall Meet. Suppl., 401, 1992.

Page, B. M., Tectonic setting of the San Francisco Bay Region, in *Proceedings on the Second Conference on Earthquake Hazards in the eastern San Francisco Bay Area*, edited by G. Borchardt, *Spec. Publ. Calif. Div. Mines Geol.*, *113*, 1–7, 1992.

Rice, J. R., Fault stress states, pore pressure distributions, and the weakness of the San Andreas Fault, in *Fault Mechanics and Transport Properties of Rocks: A Festschrift in Honor of W. F. Brace*, edited by B. Evens and T. Wong, pp. 475–503, Academic, San Diego, Calif., 1992.

Ross, D. C., The Salinian Block: A Mesozoic granite orphan in the

California Coast Ranges, in *Mesozoic Paleogeography of the Western United States, Pac. Coast Paleogeogr. Symp. 2*, edited by D. G. Howell and K. A. McDougall, pp. 509–522, Pac. Sect., Soc. of Econ. Paleontol. and Minerol., Los Angeles, Calif., 1978.

Sibson, R. H., A note on fault reactivation, *J. Struct. Geol.*, *7*, 751–754, 1985.

Sleep, N. H., and M. L. Blanpied, Creep, compaction and the weak rheology of major faults, *Nature*, *359*, 687–692, 1992.

Taylor, C. L., J. C. Cummings, and A. P. Ridley, Discontinuous en echelon faulting and ground warping, Portola Valley, California, in *Studies of the San Andreas Fault Zone in Northern California*, edited by R. Streitz and R. W. Sherburne, *Spec. Rep. Calif. Div. Mines Geol.*, *140*, 59–70, 1980.

Thurber, C. H., Local earthquake tomography: Velocities and Vp/Vs—theory, in *Seismic Tomography: Theory and Practice*, edited by H. M. Iyer and K. Hirahara, pp. 663–683, Chapman and Hall, New York, 1993.

Vidale, J. E., Finite-difference calculation of traveltimes in three dimensions, *Geophysics*, *55*, 521–526, 1990.

Wakabayashi, J., and E. Moores, Evidence for collision of the Salinian block with the Franciscan subduction zone, California, *J. Geol.*, *96*, 245–253, 1988.

Williams, S. D. P., Current motion on faults of the San Andreas system in central California inferred from recent GPS and terrestrial survey measurements, Ph.D. thesis, 250 pp., Univ. of Durham, England, 1995.

Zoback, M. D., and G. C. Beroza, Evidence for near-frictionless faulting in the 1989 (*M* 6.9) Loma Prieta, California, earthquake and its aftershocks, *Geology*, *21*, 181–185, 1993.

Zoback, M. D., et al., New evidence on the state of stress of the San Andreas fault system, *Science*, *238*, 1105–1111, 1987.

T. Parson and M. L. Zoback, U.S. Geological Survey, MS 999, 345 Middlefield Road, Menlo Park, CA 94025. (e-mail: tparsons@octopus.wr.usgs.gov)